14th IEA Heat Pump Conference
15-18 May 2023, Chicago, Illinois

Investigation of the performance of a ground-coupled CO_2 heat pump for space and water heating

Thor Alexis Sazon[a*], Homam Nikpey[a]

[a]University of Stavanger, Kjell Arholms gate 41, Stavanger 4021, Norway

Abstract

A parametric investigation on a ground-coupled CO_2 heat pump for space and water heating was performed using a model developed with Modelica. The CO_2 heat pump, with a tripartite gas cooler configuration, was modeled using the Thermal Systems library and then calibrated with experimental data, while the Borehole Heat Exchangers (BHEs) were modeled using the MoBTES library and sized following the ASHRAE methodology. Different design and operating parameters were varied to see their effects on the system's coefficient of performance (COP). Simulations showed that there is an optimal high-side pressure that maximizes the COP. The evaporator's water-side mass flow, the BHE's length, the grout's thermal conductivity, and the compressor speed all have an inverse relationship with the COP, while the low-side pressure of the heat pump and the valve's throttle area are directly related to it. However, changing these parameters to increase the COP has limits because doing so decreases the amount of heat that the system can deliver. This study serves as a starting point for the design and optimization of a bigger system that utilizes other low-temperature resources with the CO_2 heat pump.

Selection and/or peer-review under the responsibility of the organizers of the 14th IEA Heat Pump Conference 2023.

Keywords: trans-critical CO_2 heat pump; borehole heat exchanger; Modelica; Space and water heating

1. Introduction

Heating/cooling accounts for around 50% of the total energy consumption in Europe, the majority of which (~45%) comes from the residential sector [1]. Burning fuels just to provide for the thermodynamically-lower grade demands of space and water heating, which only requires ~40 - 80 °C, is highly inefficient. It wastes the thermodynamic potential of combustible fuels, resulting in large exergy losses, and leads to emissions that could have been avoidable [2]. Heat pumps are devices that can harness heat from low-temperature resources and increase it to useful temperature levels. Given the substantial consumption associated with residential heating, displacing the inefficient use of combustible fuels through heat pumps, which also promotes the use of diversified and local energy resources, can contribute to increasing energy security and to decreasing CO_2 emissions.

Most heat pumps nowadays operate through a sub-critical vapor-compression cycle that uses Hydrofluorocarbons (HFCs) as working fluid. HFCs replaced the once widely-used ozone-depleting Chlorofluorocarbons (CFCs) because they exhibited similarly good performance, efficiency, low toxicity, and non-flammability. However, they were later discovered to be very potent greenhouse gases. Recent initiatives seem to point out the inevitable phase-out of HFCs. The EU's F-gases regulation (EC517/2014) aims to gradually decrease the usage of important fluorinated gases in the EU, such as R404A, R410A, R407C, and R134a to one-fifth of 2014 in 2030 [3]. In addition, in January 2019, the Kigali amendment to the Montreal Protocol, wherein several countries committed to cutting the production and consumption of HFCs by more than 80% over the next 30 years, entered into force [4].

* Corresponding author. Tel.: +47-51-832534
E-mail address: thor.a.sazon@uis.no

The growing environmental concerns about the use of conventional synthetic heat pump refrigerants have revived the interest in natural working fluids. Carbon dioxide is one of the few non-toxic and non-flammable natural refrigerants that have zero effect on ozone layer destruction and a substantially lower global warming potential (GWP) relative to commercially available alternatives [5]. Lorentzen first proposed the modern use of CO_2 in a trans-critical heat pump cycle [6]. One of the notable configurations of the CO_2 heat pump includes the tri-partite gas cooler, first proposed by Stene [7], [8], as a way to allow simultaneous and separate production of space heating and domestic hot water in an integrated design that simplifies the heat pump layout and piping requirements.

Due to substantial irreversibility during compression and gas cooling, the performance of a CO_2 heat pump is generally lower than that of a system using a subcritical cycle [9]. In addition, the reliability of the system is not as good because of the large performance variations with operating conditions. One of the ways to improve the performance of the CO_2 heat pump is by integrating it with borehole heat exchangers (BHEs). Generally, ground temperature down to depths of 5 - 10 m is influenced by solar radiation and ambient air temperature. Below 15 m, the ground temperature remains undisturbed by seasonal temperature variations [2], [10]. The undisturbed ground temperature then increases with depth due to the heat from within the Earth's core [11]. Stable temperatures on the ground provide a more reliable heat pump performance as compared to using air as the heat source, given that air temperature varies greatly with the weather. Vertical BHEs are usually around 50-150 m in depth and may have a single U-type, double U-type, or coaxial configuration [12].

Wang et al. [13] compared the performance of a CO_2 trans-critical heat pump system that uses a U-tube BHE with the performance of conventional R22 and R134a systems. Their results suggest that if the system is applied for space conditioning and tap water heating, where high water temperature is desired, then it could reach efficiencies similar to that of a conventional R134a cycle. Kim and Chang [14] focused on the development of a model that could perform a steady-state thermodynamic performance analysis of a CO_2 geothermal heat pump system that implements a suction gas heat exchanger (SGHX). The model was implemented in Digital Visual Fortran with the graphical user interface (GUI) implemented in Visual Basic. Their simulations indicated that, in cooling mode, the COPs of the cycle with SGHX were 2-6% better than the typical trans-critical CO_2 heat pump cycle COPs. However, in heating mode, the configuration that uses an SGHX got slightly smaller COPs than those of the basic cycle. Kim et al. [9] performed a simulation study of a hybrid solar-geothermal CO_2 heat pump system for residential space heating in the winter. They considered a system configuration where heat from both the solar collector and heat pump is collected in a thermal energy storage tank whose temperature is controlled at a designated level. Engineering Equation Solver (EES) was used to model the system components and calculate the thermodynamic properties of the refrigerant. This study is also limited to steady-state performance calculations.

Replacing HFCs with alternative refrigerants requires systems with comparable efficiencies. If the new system has significantly lower efficiency and if the electricity that runs the compressor is mainly generated with the use of fossil fuels, the replacement of the existing system will just contribute more to global warming [15]. To push for wider technology uptake, careful investigation of the effects of various design and operating conditions on the performance and operating characteristics of the system is needed. Bellos and Tzivanidis [16] performed a parametric investigation on a ground-coupled CO_2 heat pump using steady-state calculations with EES. Their analysis shows the effects of ten parameters on the system's coefficient of performance, five from the heat pump and five from the BHE.

Similarly, this work performs a parametric investigation on a ground-coupled CO_2 heat pump for simultaneous space and water heating using a system model developed with the Modelica language [17]. Modelica is an equation-based, object-oriented modeling language that allows dynamic simulations. While most studies performed steady-state calculations, the model developed here can consider time-varying system characteristics, particularly the reduction of ground temperature as it is used for space and water heating. Different design and operating parameters from both the heat pump side and the BHE side were varied to see their individual effects on the system's COP. The result of this study serves as a starting point for the design and optimization of a bigger system that utilizes other low-temperature energy resources integrated with the CO_2 heat pump, and the model developed can be utilized for further simulation studies that entail time-varying inputs and responses.

2. Methods

In this work, the model was developed using Modelica with the Dymola [18] user interface. The CO_2 heat pump was modeled using the Thermal Systems library [19] in Dymola and then calibrated with experimental

data; while the BHEs were modeled using the MoBTES library [20] and then sized based on the ASHRAE methodology [21].

2.1. CO_2 heat pump modeling

The CO_2 heat pump model developed in this work was based on a 6.5 kW prototype unit constructed and tested by Stene [7, 8]. It consists of the counter-flow tripartite gas coolers, an evaporator, a compressor, a throttle valve, an SGHX, a sub-cooler, and a low-pressure receiver. Although the prototype can function in three modes (space heating only, domestic hot water (DHW) heating only, and simultaneous space and DHW heating), the model in this work was only calibrated for simultaneous space and DHW heating. Preheating of the incoming water from the supply line occurs at the first gas cooler while further increasing its temperature to a useful level is achieved at the third gas cooler. The second gas cooler separately provides the thermal energy needed for space heating.

This reference system was then converted into a Modelica model using the Thermal Systems library in the Dymola GUI. The Thermal Systems library, also synonymous with the TIL suite, is a commercial Modelica library for modeling thermo-fluid systems. It can be used to model various components, such as heat pump cycles, hydraulic networks, ventilation, and so on. It uses the TSMedia library to calculate the thermophysical properties of fluid and fluid mixtures [19].

The CO_2 heat pump model developed is shown in Fig. 1. The control strategy implemented includes: (a) controlling the DHW temperature by adjusting the water pump speed, (b) controlling the supply temperature for SH by adjusting the water pump speed, (c) controlling the high-side pressure of the heat pump by adjusting the throttle area of the valve, and (d) controlling the low-side pressure by adjusting the compressor speed. All of these were implemented in the model using proportional-integral (PI) controllers (Fig. 1).

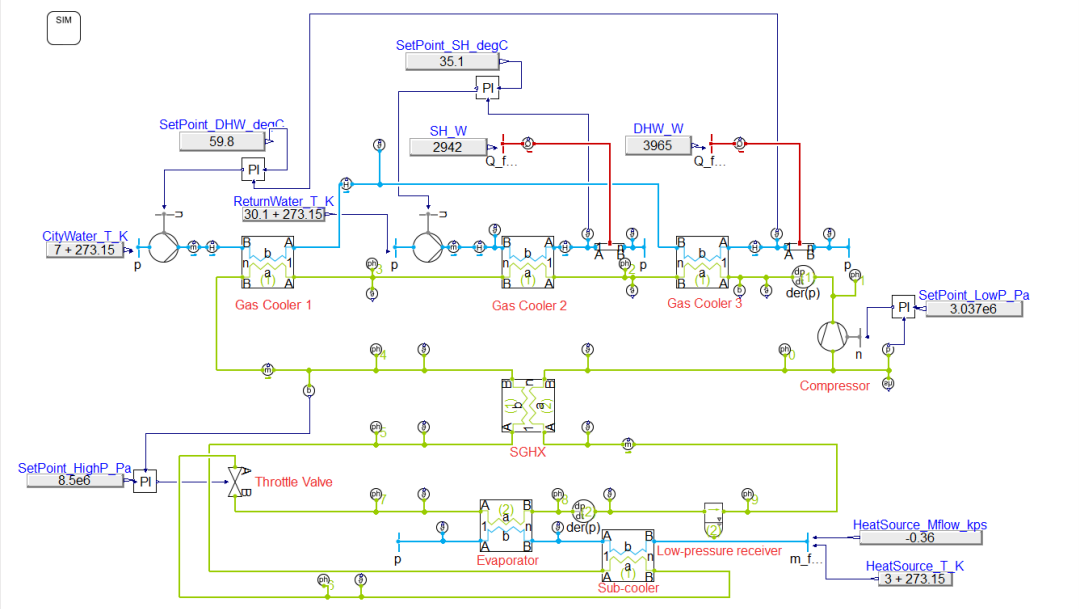

Fig. 1. CO_2 heat pump model developed in Modelica (Dymola) using the Thermal Systems library

Table 1 shows the design conditions of the prototype CO_2 heat pump unit when utilized for simultaneous space and water heating. At design conditions, the heat pump unit gives off ~3 kW of heat to a floor heating system at a supply/return temperature of 35/30 °C and ~3.5 kW to heat to the DHW from ~5 °C to ~60 °C. The compressor discharge pressure is around 85 to 90 bars, and the evaporation temperature is -5 °C. The specifications for the compressor used in the prototype are given in Table 2.

Table 1. Design conditions for the prototype CO_2 heat pump unit for simultaneous space and water heating (taken from [7])

Component	Parameter	Value
Compressor	Suction pressure (-5°C)	3.046 MPa
	Suction temperature	0°C
	Discharge pressure	8.5 to 9.0 MPa
	CO_2 mass flow rate	~1.40 kg/min
Evaporator	Evaporation temperature	-5°C
	LMTD	~5 K
Tripartite gas cooler	Space Heating (SH) -Water temperatures	35/30 °C
	SH - Heating Capacity	~3 kW
	SH - Temperature approach	<0.2 K
	DHW - Water temperatures	5/60 °C
	DHW - Heating capacity	~3.5 kW
	DHW - Temperature approach	<3 K

Table 2. Specifications for the rolling piston compressor (prototype) (taken from [7])

Type	Hermetic two-stage rolling piston unit operated as a single-stage unit (LP + HP)
Operating range	1800 to 7200 rpm (39 to 120 Hz)
Displacement volume	3.33 cm^3/rev (LP) and 1.88 cm^3/rev (HP)
Swept volume	1.439 m^3/h at 7200 rpm
Max operating pressure	14 MPa
Max discharge temperature	125 °C
Motor type	Digitally controlled brushless motor – 4 poles
Maximum power input	2500 W

During the calibration of the CO_2 heat pump, the mass flow and temperature of the BHE fluid (propylene glycol) entering the evaporator were fixed at 0.36 kg/s and 3°C, respectively. These were assumed using some rule of thumb given in the ASHRAE handbook [21] since this information was not available in the reference material used.

The measured data for the design condition at 85 bars were used to calibrate the model. The information available in Stene's work [7] was used to set the values of some parameters in the different component models, including the tube diameters of all the tube-in-tube heat exchangers, as well as their weights, material of construction, and length; the size of the low-pressure receiver; and the compressor displacement and operating range. The parameters adjusted during calibration include (a) the coefficient of heat transfer in each heat exchanger and (b) the isentropic and overall efficiencies of the compressor. A compressor model with fixed efficiencies was utilized for simplicity.

2.2. BHE modeling and sizing

Fig. 2 shows the BHE model developed in Dymola using the MoBTES library [20]. The MoBTES library is a free and open Modelica library that comprises components for the simulation of BHEs and Borehole Thermal Energy Storage (BTES) systems. It is built with objects from the Modelica Standard Library (MSL) for fluid heat flow and heat transfer. MoBTES was developed in accordance with MSL version 3.4, but in this work, it was revised to work with MSL version 4.0.

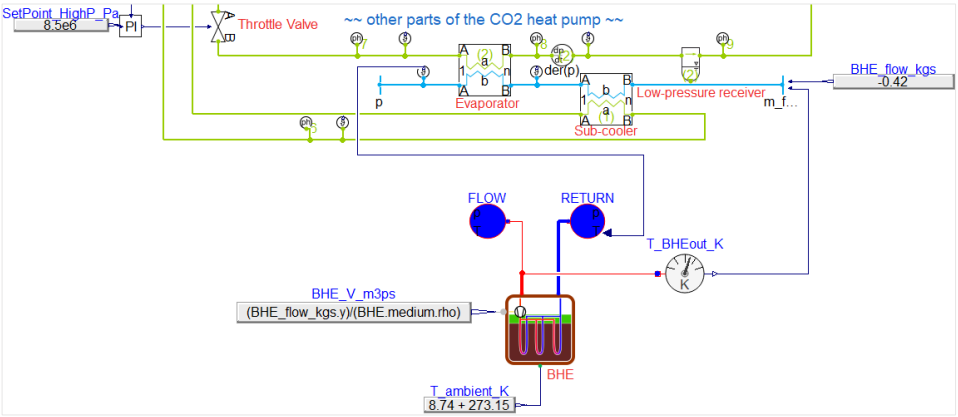

Fig. 2. The BHE model in Dymola (with a portion of the CO_2 heat pump model to show how they are connected)

The BHE was connected to the CO_2 heat pump model by considering the BHE fluid mass flow rate and temperatures. The temperature of the fluid entering the heat pump (evaporator's water side) was assumed equal to the temperature of the fluid exiting the BHE, while the temperature of the fluid exiting the evaporator's water-side was assumed equal to the temperature of the fluid entering the BHE. The mass flow rate of the fluid circulating through the BHE and the water side of the evaporator was calculated by following the ASHRAE methodology. For simplicity, the ambient temperature was fixed to a constant value equivalent to the annual average temperature in Western, Norway.

The sizing of the BHE was implemented using the ASHRAE methodology [21]. In this method, the length of the borehole required for heating purposes L_h is calculated using the Equation below.

$$L_h = \frac{Q_a R_{sa} + Q_h (R_b + PLF_m R_{sm} + F_{sc} R_{sd})}{T_0 - \frac{T_{in,hp} + T_{out,hp}}{2} - T_p} \cdot \frac{COP_h - 1}{COP_h} \quad (1)$$

Where Q_a is the net annual average heat transfer to the ground; PLF_m is the part-load factor for the design month; R_{sa}, R_{sm}, and R_{sd} are the effective thermal resistances of the ground to the annual pulse, monthly pulse, and daily pulse, respectively; F_{sc} is the short-circuit heat loss factor; R_b is the overall borehole thermal resistance; and T_p is the temperature penalty for the interference of adjacent bores.

The overall thermal resistance R_b is the sum of the heat exchanger thermal resistance R_p, which is the average of the thermal resistance of the tube R_{tube} and the film thermal resistance of the fluid R_{film}, and the thermal resistance of the grout R_{grt}.

$$R_b = R_p + R_{grt} \quad (2)$$

$$R_p = \frac{R_{tube} + R_{film}}{2} \quad (3)$$

$$R_{film} = \frac{1}{\pi d_{in} h_f} \quad (4)$$

$$R_{tube} = \frac{ln \frac{d_{out}}{d_{in}}}{2\pi k_{tube}} \quad (5)$$

$$R_{grt} = \left(k_{grt} b_0 \left[\frac{d_p}{d_{out}} \right]^{b_1} \right)^{-1} \quad (6)$$

Where d_{in}, d_{out}, and d_p are the inner, and outer diameters of the tube, and the borehole diameter, respectively; h_f is the convective heat transfer of the fluid; k_{tube} and k_{grout} are the conductive heat transfer coefficients of the tube and the grout, respectively; and b_0 and b_1 are coefficients found in the ASHRAE handbook specific to the position of the tube in the borehole.

The heat transfer coefficient of the fluid h_f is calculated using the Colburn equation [22]. In this work, the Reynold's number Re has values in the turbulent regime, so it follows that:

$$Nu = 0.023 Re^{0.08} Pr_f^{1/3} \quad (7)$$

$$Nu = h_f d_{in}/k_f \quad (8)$$

$$Re = 4m_{f,0}/\pi d_{in}\mu_f \quad (9)$$

$$Pr_f = \mu_f c_{p,f}/k_f \quad (10)$$

Where Nu is the Nusselt number; Pr is the Prandtl number; k_f is the thermal conductivity of the fluid; $m_{f,0}$ is the mass flow of the geothermal fluid in one borehole; μ_f is the fluid viscosity; and $c_{p,f}$ is the geothermal fluid heat capacity.

2.3. Parametric simulation runs

The parametric investigation was implemented by varying the values of chosen parameters one at a time. Table 3 shows the heat pump and BHE parameters varied, with their default values and the ranges of the variations implemented. Five of these parameters pertain to the heat pump and the other three pertain to the BHE. During these simulation runs, the space and water heating demand were fixed to the value used during the calibration simulation. The mass flow of the BHE fluid was also fixed to the value calculated from the ASHRAE methodology (0.42 kg/s). Each simulation case was run for 980 hours [21]. Note that this only covers the full load hours in a year. Since the COP of the system changes with time, given that the input temperature of the heat source changes with utilization, only the COP values at the end of the simulation time were compared.

Table 3. Parameters varied during the parametric analysis

Parameter Varied	**Default Value**	**Range of variation**
Heat pump high-side pressure, bar	85	77 - 100
Heat pump low-side pressure, bar	30.37	29.69 - 31
Throttle valve area, $x10^{-7}$ m^2*	2.5	2.1 - 2.7
Compressor speed, Hz*	115	108 - 120
Evaporator water-side flow rate, kg/s	0.42	0.3 - 0.5
BHE length, m	95	85 - 110
BHE spacing, m	6	3 - 10
Grout thermal conductivity, W/m-K	1.5	1 - 5

**Varying these parameters requires the removal of the high- and low-side pressure controllers*

3. Results and discussions

In this work, the model was developed using Modelica with the Dymola [18] user interface. The CO_2 heat pump was modeled using the Thermal Systems library [19] in Dymola and then calibrated with experimental data; while the BHEs were modeled using the MoBTES library [20] and then sized based on the ASHRAE methodology [21].

3.1. Calibration of the CO_2 heat pump model

The heat pump model was calibrated using the measured data at the high-side pressure of 85 bars; this represents the design conditions of the heat pump. Some component specifications were obtained from the reference material while some were determined through the calibration process. Table 4 shows the values of the heat exchanger parameters whileTable 5 shows the parameters for the other heat pump components, such as the low-pressure receiver and the compressor. During calibration, the values of the heat transfer coefficients were assumed equal for the two sides of each heat exchanger and then adjusted so that the heat flows and the available inlet/outlet temperatures (Table 1 (water) and Table 6 (CO_2)) and temperature approach data (Table 1) are matched. Some of them required to have different water-side and CO_2-side heat transfer coefficients to match the data. The efficiencies of the compressor were adjusted to simulate measured heat flows, power consumption and CO_2 inlet temperature. The effective isentropic efficiency (Table 4) also takes into account the supplied mechanical power.

Table 4. CO_2 heat pump heat exchanger specifications

	Gas Cooler 1	**Gas Cooler 2**	**Gas Cooler 3**	**Evaporator**	**Sub-cooler**	**SGHX**
CO_2-side tube length, m	14	15	3.5	12	6	2.3
CO_2-side tube inner diameter, m	0.006	0.006	0.006	0.008	0.008	0.08/0.12
CO_2-side heat transfer coefficient, W/m^2-K*	9000	7000	3500	6500	150	550
Water-side tube length, m	14	15	3.5	12	1	NA
Water-side tube inner diameter, m	0.012	0.018	0.012	0.02	0.025	NA
Water-side heat transfer coefficient, W/m^2-K*	9000	7000	5500	4500	150	NA
Wall thermal resistance, K/W (Stainless Steel)	0.00025	0.00025	0.00025	0.00025	0.0001538	0.00025
Mass, kg	13	18	6	17	17	2.5

**Values determined from the calibration process*

Table 5. Other CO_2 heat pump component specifications

Compressor		
Displacement, m^3	3.33x10^{-06}	
Volumetric Efficiency*	0.85	
Isentropic Efficiency	0.8	
Effective Isentropic Efficiency*	0.62	
Pumps	DHW	SH
Volume of liquid in pump, m^3	1.60x10^{-05}	1.00x10^{-04}
Volumetric flow rate at nominal speed, m^3/s	6.00x10^{-05}	6.00x10^{-05}
Pressure increase at 0 flow, bar	2	2
Speed, Hz	5 - 150	5 - 150
Nominal efficiency	0.4	0.4
Low-pressure receiver		
Volume, m^3	0.004	
Initial filling level	0.5	

**Values determined from the calibration process*

Table 6 gives the results of the CO_2 heat pump calibration runs. The model was calibrated against the data for P_{GC} = 85 bars, while the other measured data were used to test the calibrated model. Calibration and test errors were obtained by comparing the measured and simulated COPs. As shown, the error generated by the calibrated model increases when it is used to simulate an off-design condition (design conditions: 85 to 90 bars, as given in Table 1). This can be partly attributed to the choice of using a simplified compressor model that assumes constant efficiencies.

Table 6. Results of the calibration CO_2 heat pump unit at ~60°C DHW temperature, ~35/30°C supply /return temperature for SH (data taken from [7]; $Q_{DHW} = Q_{GC1} + Q_{GC3,} Q_{GC2}$ is the heat for SH, T_E is the evaporator temperature in the CO_2 loop)

Data type	**P_{GC}, bars**	**T_E, °C**	**Q_{GC}, W**	**Q_{DHW}, W**	**Q_{GC1}, W**	**Q_{GC2}, W**	**Q_{GC3}, W**	**Power$_C$, W**	**Tin/out$_{CO2_GC}$, °C**	**$M_{CO2,}$ kg/s**	**COP**	**Error**
Measured*	85	-5.1	6907	3965	1608	2942	2357	1775	86.40/9.80	1.441	3.89	-0.26%
Calibrated	85	-5.1	6710	3776	1534	2934	2242	1730	86.56/9.80	1.449	3.88	
Measured*	89.8	-5	6947	4351	1550	2596	2801	1878	90.60/8.50	1.442	3.70	1.89%
Simulated	89.8	-5	6711	4074	1480	2637	2594	1779	90.76/8.17	1.417	3.77	
Measured	80.3	-5.1	6230	3502	1674	2728	1828	1699	81.60/18.00	1.440	3.67	4.90%
Simulated	80.3	-5.1	6595	3615	1707	2981	1907	1715	83.82/15.41	1.500	3.85	

**Design conditions*

3.2. Modeling and sizing of the BHE

The parameters assumed to calculate the size of the BHE using the ASHRAE methodology are given in Table 7. As shown, it was assumed that 4 BHEs are needed to provide the ~6.5 - 7 KW heat required by the system. A yearly equivalent heating full-load hours of 980 h then was assumed based on the data given in the ASHRAE handbook for Portland, Maine [21], assuming that the weather there is comparable to that of western Norway. The ground was assumed to have the characteristics of Slate, one of the common rock types in some parts of Norway [23] while the thermal gradient was assumed to be 0.0125 K/m, similar to that of some wells drilled in Bergen, Norway [24].

Following the procedure in the ASHRAE method, a borehole length of 82 m/well was calculated. Consequently, the calculated BHE length, as well as the assumed BHE parameters, were inputted to the BHE model, and a simulation was run to see if it can maintain the output of the heat pump system to around 6.7 kW (value used in the calibration) for the equivalent full-load hours of 980 h.

The result of the simulation shows that a BHE length of 82 m was not enough to maintain the output of the heat pump system to at least 6.7 kW for 980 h of continuous operation. Of course, in reality, the heat pump is not expected to be operated continuously for 980 h at full load, so this BHE length might already be enough for the expected usage. However, it is normal to oversize the BHE to take into account the changes in the performance that can be expected from the changes in ground temperature upon utilization [25]. Therefore, the BHE length was increased until simulation shows that it can support at least 6.7 kW by the end of 980 h of continuous full-load run. From this, a borehole length of 95 m was determined and used as the base value for the parametric simulation runs.

Table 7. BHE parameters

BHE parameter	Value
Average ambient temperature, °C	7
Geothermal gradient, K/m	0.0125
Ground density, kg/m^3	2760
Ground specific heat, J/kg-K	920
Ground thermal conductivity, W/m-K	2.1
Layout	Rectangle
BHE type	Single U
Number of BHEs	4
Borehole diameter, m	0.15
Tube inner diameter, m	0.034
Tube thickness, m	0.003
Tube thermal conductivity, W/m-K	0.4
Shank spacing, m	0.08
Number of BHE in series	1
Grout density, kg/m^3	1900
Grout thermal capacity, J/kg-K	1300
Grout thermal conductivity, W/m-K	1.5
Calculated BHE length, m/well*	82
Adjusted BHE length, m/well**	95

**Calculated using the ASHRAE method **Determined through simulation*

3.3. Parametric Simulation Runs

Simulation runs were performed to see the effects of varying some of the heat pump and BHE design and operating parameters on the COP (Table 3). Before the parametric runs, the performance of the base model, which uses the default values of the parameters, was determined. Fig. 3 shows the COP, the heat extracted from the BHE, the total heat from the gas coolers, and the power input to the compressor with the time of the base model. It can be seen that the heat derived from the BTES and consequently from the gas coolers decreased with time. This is expected as thermal energy from the ground, as well as its temperature (Fig. 4), would decrease if it were continuously used to provide the heating demand without recharge. Nonetheless, the

COP throughout the full-load period of 980 h remained between 3.8 and 4.

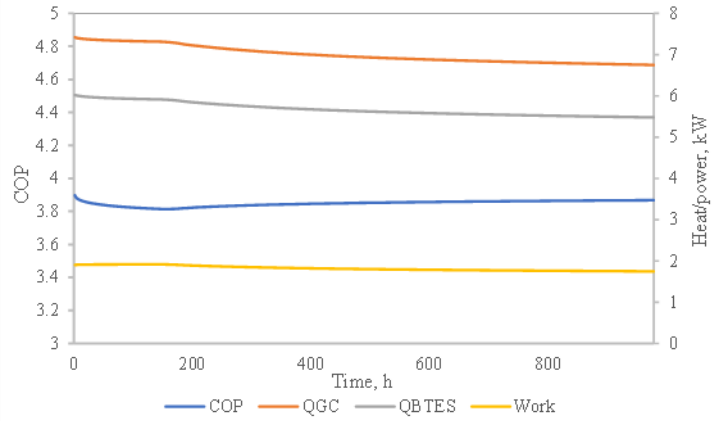

Fig. 3. Performance of the base model with time

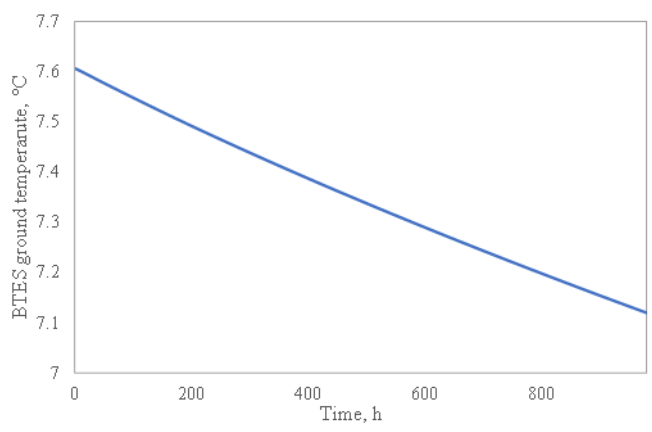

Fig. 4. Ground temperature with time

Fig. 5 gives the results of the parametric simulation runs. To make the comparison easier, only the performance values at the end of the 980 h simulation runs were used. It should be noted that the variation in the compressor speed and throttle valve area were both implemented by removing the PI controllers that maintain the high-side and low-side pressure at fixed levels. This means that for these two sets of simulation runs, the high- and low-side pressure varies with the parameter variation, unlike in the other parametric simulation runs performed here. Stene [7] pointed out that the high-side pressure of the CO_2 heat pump is controlled by using the low-pressure receiver and by adjusting the opening of the expansion valve, which temporarily changes the balance between the mass flow rate in the compressor and the valve. Reducing the valve opening accumulates more CO_2 in the gas cooler piping, thereby increasing the high-side pressure until a new balance point for the mass flow rate in the compressor and the valve is reached. The extra CO_2 charge needed to increase the pressure is boiled off from the liquid reservoir in the receiver. On the other hand, opening the expansion valve reduces the high-side pressure and the surplus CO_2 is stored as a liquid in the receiver.

It can be seen from Fig. 5a that an optimum high-side pressure that maximizes the COP of the system is present. In this case, it occurs at the design operating pressure of 85 bars. The compressor speed, the evaporator's water-side mass flow, the BHE's length, BHE spacing, and the grout's thermal conductivity all have an inverse relationship with the COP. However, as any of these parameters were lowered to increase the COP, the amount of heat that the system can deliver also decreased. This points out that they can only be decreased to certain limits when they could still sufficiently provide the value of the heat demand. On the other hand, as the low-side pressure of the heat pump and the throttle valve area were increased, the COP also increased. Similarly, there are also limits on these since increasing their respective values decreases the heat that could be delivered by the system.

Given the assumed variation range of the parameters, it can also be observed that the performance of the heat pump is most reactive to the high-side (discharge) heat pump pressure and the throttle vale area, followed

by the low-side (suction) heat pump pressure and the compressor speed. Conversely, it is least reactive to the variation in the BHE spacing and the grout thermal conductivity.

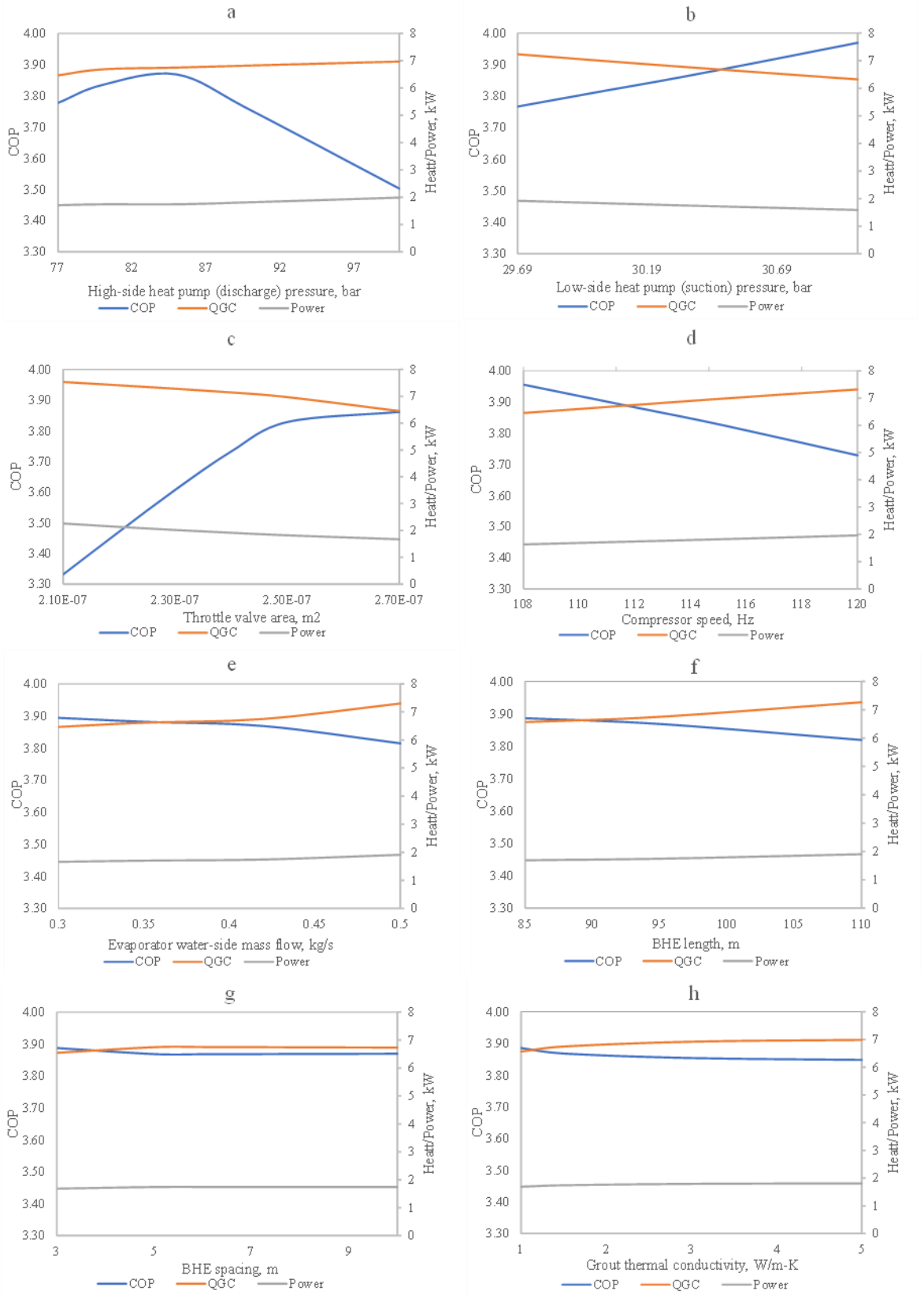

Fig. 5. Variation of COP with different heat pump and BHE parameters: (a) high-side pressure, (b) low-side pressure, (c) throttle valve area, (d) compressor speed, (e) evaporator water-side mass flow rate, (f) BHE length, (g) BHE spacing, and (h) grout thermal conductivity

4. Conclusion

A parametric analysis was performed on a ground-coupled CO_2 heat pump system that is designed to simultaneously provide for both space and water heating demands. The CO_2 heat pump model was first developed and calibrated using data from an experimental setup. Afterward, the BHE was modelled and then sized using the ASHRAE methodology.

The calibration shows that the model performs closely to the experimental rig when it operates within design conditions. The results of the parametric studies show that an optimum high-side pressure maximizes the COP of the system. The compressor speed, the evaporator's water-side mass flow, the BHE's length, and the grout's thermal conductivity all have an inverse relationship with the COP, while the low-side pressure of the heat pump and the throttle area of the expansion valve are directly related to it. However, changing all these parameters to increase the COP has limits since they all impose a decrease in the amount of heat that can be delivered by the system. It was also observed that the performance of the heat pump is most reactive to the high-side (discharge) heat pump pressure and the throttle vale area, followed by the low-side (suction) heat pump pressure and the compressor speed. Conversely, it is least reactive to the variation in the BHE spacing and the grout thermal conductivity.

This work is planned to be further extended to investigate other performance indicators, such as the total annual cost, seasonal performance factor, and ground temperature change. It is also planned to expand the system to include a solar thermal collector component, a tank thermal energy storage, and energy demand specifications that follow realistic patterns for a given year.

Acknowledgments

This paper is part of the Ph.D. work funded internally by the University of Stavanger.

References

[1] European Commission, An EU Strategy on Heating and Cooling. 2016. Accessed: May 23, 2022. [Online]. Available: https://eur-lex.europa.eu/legal-content/EN/TXT/?qid=1575551754568&uri=CELEX:52016DC0051

[2] T. Sliwa and M. A. Rosen, "Natural and Artificial Methods for Regeneration of Heat Resources for Borehole Heat Exchangers to Enhance the Sustainability of Underground Thermal Storages: A Review," Sustainability, vol. 7, no. 10, Art. no. 10, Oct. 2015, doi: 10.3390/su71013104.

[3] "EU legislation to control F-gases." https://ec.europa.eu/clima/eu-action/fluorinated-greenhouse-gases/eu-legislation-control-f-gases_en (accessed Apr. 01, 2022).

[4] United Nations, "The Kigali Amendment (2016): The amendment to the Montreal Protocol agreed by the Twenty-Eighth Meeting of the Parties (Kigali, 10-15 October 2016) | Ozone Secretariat," 2016. https://ozone.unep.org/treaties/montreal-protocol/amendments/kigali-amendment-2016-amendment-montreal-protocol-agreed (accessed Mar. 18, 2021).

[5] R. U. Rony, H. Yang, S. Krishnan, and J. Song, "Recent Advances in Transcritical CO2 (R744) Heat Pump System: A Review," Energies, vol. 12, no. 3, Art. no. 3, Jan. 2019, doi: 10.3390/en12030457.

[6] G. Lorentzen, "Trans-critical vapour compression cycle device," WO1990007683A1, Jul. 12, 1990 Accessed: Feb. 17, 2021. [Online]. Available: https://patents.google.com/patent/WO1990007683A1/en

[7] J. Stene, Residential CO2 Heat Pump System for Combined Space Heating and Hot Water Heating. Fakultet for ingeniørvitenskap og teknologi, 2004. Accessed: May 23, 2022. [Online]. Available: https://ntnuopen.ntnu.no/ntnu-xmlui/handle/11250/233381

[8] J. Stene, "Residential CO2 heat pump system for combined space heating and hot water heating," International Journal of Refrigeration, vol. 28, no. 8, pp. 1259–1265, Dec. 2005, doi: 10.1016/j.ijrefrig.2005.07.006.

[9] W. Kim, J. Choi, and H. Cho, "Performance analysis of hybrid solar-geothermal CO2 heat pump system for residential heating," Renewable Energy, vol. 50, pp. 596–604, Feb. 2013, doi: 10.1016/j.renene.2012.07.020.

[10] S. Gehlin, "Thermal response test: method development and evaluation," Doctoral Thesis, Luleå University of Technology, Luleå, Sweden, 2002. [Online]. Available: http://www.diva-portal.org/smash/get/diva2:991442/FULLTEXT01.pdf

[11] D. Banks, An Introduction to Thermogeology: Ground Source Heating and Cooling. John Wiley & Sons, 2009.

[12] G. Florides and S. Kalogirou, “Ground heat exchangers—A review of systems, models and applications,” Renewable Energy, vol. 32, no. 15, pp. 2461–2478, Dec. 2007, doi: 10.1016/j.renene.2006.12.014.
[13] J. Wang, L. Kang, and J. Liu, “CO2 Transcritical Cycle for Ground Source Heat Pump,” in 2009 WRI World Congress on Computer Science and Information Engineering, Mar. 2009, vol. 2, pp. 213–217. doi: 10.1109/CSIE.2009.235.
[14] Y.-J. Kim and K.-S. Chang, “Development of a thermodynamic performance-analysis program for CO2 geothermal heat pump system,” Journal of Industrial and Engineering Chemistry, vol. 19, no. 6, pp. 1827–1837, Nov. 2013, doi: 10.1016/j.jiec.2013.02.028.
[15] S. Riffat, D. Aydin, R. Powell, and Y. Yuan, “Overview of working fluids and sustainable heating, cooling and power generation technologies,” International Journal of Low-Carbon Technologies, vol. 12, no. 4, pp. 369–382, Dec. 2017, doi: 10.1093/ijlct/ctx008.
[16] E. Bellos and C. Tzivanidis, “Parametric Investigation of a Ground Source CO2 Heat Pump for Space Heating,” Energies, vol. 14, no. 12, Art. no. 12, Jan. 2021, doi: 10.3390/en14123563.
[17] Modelica Association, “Modelica Language,” 2021. https://modelica.org/modelicalanguage.html (accessed Sep. 02, 2021).
[18] Dassault Systèmes, “Dymola,” 2022. https://www.3ds.com/products-services/catia/products/dymola/ (accessed May 23, 2022).
[19] Claytex Technia Company, “Thermal Systems Library & TIL Suite,” Claytex, 2022. https://www.claytex.com/products/dymola/model-libraries/thermal-systems-library/ (accessed May 23, 2022).
[20] J. Formhals, H. Hemmatabady, B. Welsch, D. O. Schulte, and I. Sass, “A Modelica Toolbox for the Simulation of Borehole Thermal Energy Storage Systems,” Energies, vol. 13, no. 9, Art. no. 9, Jan. 2020, doi: 10.3390/en13092327.
[21] S. P. Kavanaugh and K. D. Rafferty, Geothermal Heating and Cooling: Design of Ground-source Heat Pump Systems. ASHRAE, 2014.
[22] A. P. Colburn, “A method of correlating forced convection heat-transfer data and a comparison with fluid friction,” International Journal of Heat and Mass Transfer, vol. 7, no. 12, pp. 1359–1384, Dec. 1964, doi: 10.1016/0017-9310(64)90125-5.
[23] J. Stene, “Ground-source heat pump systems in Norway IEA HPP Annex 29 (2004-2006),” Norway, NEI-NO--0706407, 2007. [Online]. Available: https://inis.iaea.org/search/search.aspx?orig_q=RN:38097084
[24] K. Midttømme, “Geothermal Energy in Norway and Hordaland,” Bergen Energy Lab, 06 2017. [Online]. Available: https://www.uib.no/en/energy/108628/kirsti-midtt%C3%B8mme-geothermal-energy-norway-and-hordaland
[25] T. Persson, O. Stavset, R. K. Ramstad, M. J. Alonso, and K. Lorenz, “Software for modelling and simulation of ground source heating and cooling systems,” SINTEF Energy Research, Trondheim, Norway, TR A7570, 2016. Accessed: Feb. 17, 2021. [Online]. Available: https://www.sintef.no/globalassets/sintef-energi/interact/tr-a7570-software-for-modelling-and-simulation-of-ground-source-heating-and-cooling-systems-2016.pdf